Journal of Carcinogenesis
Covering Genesis to Therapeutics

Journal of Carcinogenesis, ISSN: 1477-3163
2025; Vol 24: Issue 7s, https://carcinogenesis.com/

# Multi-Head Probsparse Spherical Convolutional Network With Lyrebird Optimization Algorithm For Prostate Cancer Identification

**K. Ramakrishna Reddy[1], Dr. Ratnakirti Roy[2]**

[1]Ph.D Research Scholar, Visvesvaraya Technological University, Belagavi, Assistant Professor, Department of Computer Application, Acharya Institute of Graduate Studies, Bangalore.

Email ID: kundur1985@gmail.com

[2]Associate Professor and Head, Department of Computer Application, Acharya Institute of Technology, Banaglore.

## ABSTRACT

Prostate cancer remains a leading cause of mortality among men worldwide, and accurate early detection is critical for improving treatment outcomes. Traditional diagnostic methods and conventional imaging analyses often suffer from low Accuracy, high inter-observer variability, and limited capacity to capture complex tissue structures in MRI images. To address these limitations, this study proposes a novel Multi-Head ProbSparse Spherical Convolutional Network with Lyrebird Optimization Algorithm (M-HPSCNet-LOA) for prostate cancer identification from the SPIE-AAPM-NCI Prostate dataset using MRI images. The framework incorporates Deep Attentional Guided Image Filtering (DAGIF) for pre-processing, Single-Head Vision Transformer (SHViT) for segmentation, and Dimba: Transformer-Mamba Diffusion Models (TMDM) for feature extraction. Classification is achieved through the Multi-Head ProbSparse Spherical Convolutional Network (MHPSCNet), which integrates Multi-Head ProbSparse Self-Attention (MHPSAN) and Spherical Convolutional Neural Network (SCNN) to capture both global tissue structures and localized intensity patterns. The Lyrebird Optimization Algorithm (LOA) further enhances model performance by fine-tuning parameters efficiently. Experimental results demonstrate that M-HPSCNet-LOA achieves 99.85% accuracy, 99.58% F1-score, and 99.62% precision, highlighting its robustness, stability, and applicability in MRI-based prostate cancer detection.

***Keywords:*** *Deep Attentional Guided Image Filtering, Lyrebird Optimization Algorithm, Multi-Head Probsparse Self-Attention, Spherical Convolutional Neural Network, Single-Head Vision Transformer.*

**How to Cite:** K. Ramakrishna Reddy1, Dr. Ratnakirti Roy, (2025) Multi-Head Probsparse Spherical Convolutional Network With Lyrebird Optimization Algorithm For Prostate Cancer Identification, *Journal of Carcinogenesis*, *Vol.24, No.7s*, 726-737

## 1. INTRODUCTION

Pathological grading is crucial for prostate cancer (PCa) risk evaluation and therapy selection. PCa is traditionally diagnosed by taking systematic core needle biopsies across the prostate gland[1-3]. As a result, the number of new cases expected each year could reach 25 million by 2030[4-6]. Prostate cancer rates that survive can be considerably raised over the existing rate, and the right kind of intervention can be given if it can be accurately identified in its early stages[7-10]. This type of MRI, which can locate and visualize prostate cancer lesions, was created by combining various anatomic and clinical magnetic resonance imaging (MRI) sequences[11-12]. The Faster R-CNN models are used to classify the images, while the enhanced ResNet model is used to extract their features. The dual optimizers (Adam and SGD) are used to optimize the models' parameters, ensuring that prostate cancer can be accurately recognized[13-15]. Radiomics has made substantial use of convolutional neural networks (CNNs), which are a class of deep learning techniques that include convolutional, pooling, stimulation, and fully connected layers. CNN-built models enable deep mining of data from images by automatically learning to extract and choose visual features for use in predictions[16]. Major medical datasets and the development of algorithms for deep learning (DL) have significantly accelerated image processing and assisted pathologists in making early cancer diagnoses [17].

*Novelty and Contribution*

- DAGIF improves MRI quality by reducing noise, normalizing intensities, and enhancing anatomical consistency for reliable feature preservation.
- SHViT enables efficient segmentation by isolating prostate lesions, preserving tumor boundaries, and capturing both local and global dependencies.

- TMDM extracts robust multiscale features, balancing long-range tissue dependencies with computational efficiency for accurate cancer representation.
- MHPSCNet combines MHPSAN and SCNN to capture global tissue patterns and localized variations, improving classification accuracy and lesion detection.
- LOA optimizes parameters effectively, balancing exploration and exploitation, ensuring stable convergence, and boosting overall diagnostic performance.

The relevant literature is reviewed in detail in Section 2. A thorough explanation of the methods employed in this investigation is given in Section 3. The results are examined in Section 4. The contributor's personal opinions and recommendations for additional study are presented in Section 5.

## 2. LITERATURE SURVEY

In 2024, Sanjay Kumar Singh *et al.* [18] evaluated a deep learning framework for prostate cancer detection using Gleason grading; the framework showed excellent specificity, precision, and sensitivity across MRI volumes utilizing a three-dimensional CNN. It uses Endorectal Coil-assisted MRI to segment epithelial areas and Gleason scores, which makes it computationally demanding for full-volume analysis and dependent on specific imaging methods.

In 2024, Alparslan Horasan and Ali Gunes [19] demonstrated that prostate cancer detection from Magnetic Resonance Imaging was improved by the evaluated methodology, which used three-dimensional CNN, Residual Network (RN), and Inception Neural Network in an ensemble with soft voting. It achieved high Accuracy, sensitivity, specificity, and F1 score, but it necessitates complex model integration and substantial computational resources for clinical deployment.

In 2023, Takaaki Yoshimura *et al.* [20] analyzed a methodology that improved precision and recall by successfully predicting Gleason Score from multiparametric Magnetic Resonance Images using a three-dimensional CNN with DeepLabv3+ (Deep Laboratory Version 3 Plus) semantic division. However, overall Accuracy showed little change, and the approach necessitates a large amount of computational resources for segmentation-based analysis.

In 2024, Saleh T. Alanezi *et al.* [21] demonstrated a machine-learning approach that uses first- and second-order texture attributes in radiometric analysis to diagnose prostate cancer. Support vector machine (SVM) and random forest (RF) classifiers were used to pick features using recursive feature elimination (RFE) and least absolute shrinkage and selection operator (LASSO). Prediction was improved by combining apparent diffusion coefficient (ADC) maps with T2-weighted imaging (T2WI); however, the techniques necessitated careful hyperparameter tweaking and processing resources.

### *A. Problem statement*

Numerous methods have demonstrated encouraging results in current studies for prostate cancer detection, but they also highlight difficulties. High specificity, precision, and sensitivity were demonstrated by deep learning frameworks that use three-dimensional convolutional neural networks; however, these frameworks are computationally demanding, especially when processing entire MRI volumes, and frequently rely on specialized imaging protocols like Endorectal Coil-assisted MRI. Multiple network ensemble techniques, such as RN and Extrusion Neural Networks, increased reliability and precision but limited their immediate clinical use due to their intricate integration and high computing costs. Although semantic segmentation-based techniques improved recall and precision for predicting Gleason scores, they did not considerably increase overall Accuracy. They required a large amount of processing resources for volumetric analysis. Although they required significant processing power and careful hyperparameter tuning, radiomics-based techniques that integrated texture information from multiparametric MRI with sophisticated feature selection enhanced prediction performance. Overall, the complexity, resource intensity, and dependence on specialized imaging of these approaches limit their scalability and regular clinical application.

## 3. PROPOSED METHODOLOGY

The workflow of the proposed M-HPSCNet-LOA begins with MRI data acquisition from the SPIE-AAPM-NCI Prostate dataset. Pre-processing is performed using DAGIF to reduce noise, normalize intensity, and enhance anatomical consistency. The refined images are segmented with SHViT, which efficiently isolates prostate regions and preserves tumor boundaries. Next, TMDM is employed for feature extraction, capturing both long-range dependencies and acceptable tissue variations while maintaining computational efficiency. The extracted features are classified using MHPSCNet, which combines MHPSAN to highlight informative regions and SCNN to model spherical structural patterns, ensuring robust recognition of cancerous lesions. Finally, LOA is applied to optimize model parameters, balancing exploration and exploitation to enhance Accuracy and stability. This end-to-end process provides a highly reliable pipeline for prostate cancer detection from MRI images. The M-HPSCNet-LOA approach is illustrated in Figure 1.

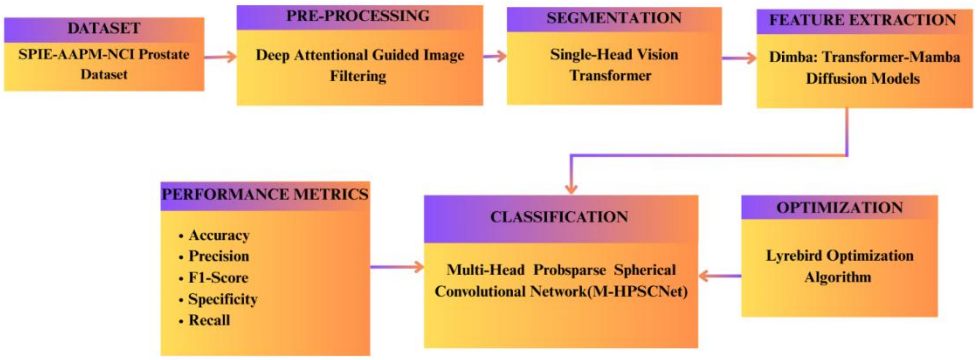


Fig.1. Block Diagram for the proposed method

*A. Data Acquisition*

The SPIE-AAPM-NCI Prostate dataset has 346 patients with PI-RADS scores ≥3. Multiparametric MRI sequences include T2-weighted, Diffusion-Weighted (DW/ADC), Dynamic Contrast-Enhanced (DCE), Proton Density-Weighted, and Ktrans images. Expert radiologists noted ground-truth lesions to aid in accurate prostate cancer detection, Gleason grading, and further classification.

*B. Pre-Processing Using Deep Attentional Guided Image Filtering (DAGIF)*

To enhance the performance of deep learning models, pre-processing entails preparing raw medical images by noise reduction, normalization, scaling, and augmentation. By altering the DAGIF[22] approach, prostate cancer detection by medical imaging can be made more reliable and perform better. Anatomical alignment, spatial resolution, and MRI intensity values are some of the patient imaging data that are suitably standardized to guarantee consistency across scans. By preserving consistency across several imaging sessions and scanners, these changes improve data integrity. Furthermore, multiscale pre-processing is used to maintain local tissue variations as well as global anatomical characteristics across pictures. Equation (1) explains how this method makes it possible to identify modest indicators of the advancement of prostate cancer.

$$G_j^g = DOWN\left(G_{j-1}^g\right), 0 < j < n \quad (1).$$

where $DOWN$ represents a downsampling method used on medical imaging to lower resolution while preserving crucial tissue and structural information, assuming that $G_j^g$ denotes an image at level $j$ in a multiscale system and that $G_{j-1}^g$ represents its previous scale. $j$ And $n$ indicates continuous scans over divided image patches. Dual Kernel Generation enables the model to capture both more general anatomical patterns and fine-grained tumor characteristics by evaluating the image data using two distinct kernels. At different image scales, this technique enhances the detection of prostate cancer markers, as explained in Equation(2).

$$X_j^g = Conv\left(Conv\left(F_j^g\right)\right), 0 \le j < n \quad (2).$$

where $X_j^g$ denotes the creation of adaptive kernels utilizing intermediate filtered image features, and $Conv\left(Conv\left(F_j^g\right)\right)$ denotes the two-step kernel development refining process during pre-processing. Adaptive Kernel Combination combines kernels from raw image data and reference anatomical patterns using an attention-driven methodology. To ensure the model focuses on trustworthy and contextually crucial features, as described in Equation (3), this technique enhances important tumor and tissue markers while reducing unnecessary noise, thereby increasing the Accuracy of prostate cancer identification across images.

$$E_j = UNet\left(\left[F_j^g, F_j^g\right]\right), 0 \le j < n \quad (3).$$

where $UNet$ indicates the module that creates the attention map, $\left[F_j^g, F_j^g\right]$ provides the corresponding image patching

at the precise same scale and Position, and $E_j$ represents the output of the attention mechanism. The learnt adaptive kernels are utilized to medium- to fine-resolution image characteristics using a guided filtering process. In this case, $n$ represents the overall number of image patches that have been processed. Equation (4) illustrates how this method reduces noise and excessive variations during pre-processing while enhancing significant anatomical and new tissue patterns.

$$Q(u,v) = \sum_{x=-\sigma}^{\sigma} \sum_{x=-\sigma}^{\sigma} Y_{v,w}(y,x) \cdot \tilde{E}(u-y, u-x) \quad (4).$$

where $\tilde{E}(u-y, u-x)$ indicates local segment variables utilized during intermediate image processing, $\sum_{y=-\sigma}^{\sigma} \sum_{y=-\sigma}^{\sigma} Y_{v,w}(y,x)$ represents a kernel-based adaptive filtering performed across surrounding regions, and $Q(u,v)$ is the final filtering output at a particular image feature. This technique enhances key anatomical features and improves the detection accuracy of prostate cancer by highlighting pertinent tumor and tissue patterns and reducing contextual noise through pre-processing. The DAGIF technique aims to enhance prostate cancer detection by improving the image quality and uniformity of medical images through multidimensional, attention-driven pre-processing that preserves significant anatomical and tumor characteristics while reducing noise and needless variations. After pre-processing, segmentation is covered in the next section.

*C. Segmentation using Single-Head Vision Transformer (SHViT)*

By dividing medical images into relevant parts, segmentation isolates organs or malignancies for accurate analysis, detection, and focused classification. To effectively capture both local and global tissue dependencies, SHViT[23] for prostate cancer classification and segmentation combines Depthwise Convolution (DWConv) for regional data aggregation with Single-Head Self-Attention (SHSA) for regional modeling. Its partial attention channel architecture improves memory efficiency, speeds up processing, and eliminates redundancy. By preserving accurate tumor borders, improving feature extraction from a range of prostate tissue intensities, and enabling reliable detection in a variety of imaging conditions, SHViT improves segmentation accuracy and classification reliability for prostate cancer lesions. Equation (5) explains how SHSA output is calculated.

$$SHSA(Y) = Concat\left(\tilde{Y}_{att}, Y_{res}\right)E^{O} \quad (5).$$

where the input feature map is denoted by $SHSA(Y)$, the attended feature map by $att$, the attention operation by $\tilde{Y}_{att}$, residual (untouched) pathways by $Y_{res}$, the output projected weighting matrix using $E^{O}$, and the concatenation merging of attended and remnant features by $Concat$. The computation of attention features for the identification of prostate cancer lesions is explained in Equation (6).

$$\tilde{Y}_{att} = Attention\left(Y_{att}E^{W}, Y_{att}E^{P}, Y_{att}E^{U}\right) \quad (6).$$

where, $Attentior$ extracts the entire context from the input features. $E^{W}$, $E^{P}$, and $E^{U}$ represent the parameter, request, and value projections weight matrices, respectively. $\tilde{Y}_{att}$ represents the chosen partial features from $Y$. The scaled dot-product attentiveness for prostate cancer image feature extraction is established by Equation (7).

$$Attention(W,P,U) = Softmax\left(WP^{L} / \sqrt{e_{gp}}\right)U \quad (7).$$

where, $W$ and $P$ are the query and key matrices, $U$ represents the value matrix, and $\sqrt{e_{gp}}$ denotes the dimension of the query or key vectors, and $Softmax$ computes normalized scores for attention using $W$. The comparable score matrix between keys and queries is represented by $WP^{L}$. The feature separation for partial attention in prostate cancer image analysis is explained by Equation (8).

$$Y_{att}, Y_{res} = Split\left(Y, [B_k, B - B_k]\right) \quad (8).$$

where $Y_{res}$ represents features that avoid attention to preserve efficiency, $B$ indicates the total number of methods, $B_k$ is the total number of characteristics used for attention, and $Y_{att}$ provides the portion of variables processed by attention.

For prostate cancer image analysis, $Split$ it stands for the division of input $Y$ according to specified sizes $B_k, B - B_k$. The SHViT aims to accurately detect and isolate prostate cancer lesions on MRI images by detecting both local and global tissue dependencies. It improves tumor boundary integrity and feature extraction, ensuring Accuracy and effective segmentation under a range of imaging conditions. After segmentation, feature extraction is covered in the next section.

*D. Feature Extraction using Dimba: Transformer-Mamba Diffusion Models (Dimba (TMDM)*

Features that indicate depth, texture, shape, and intensity are extracted from images using feature extraction, which can be done manually or automatically. The Dimba (TMDM)[24] architecture combines Mamba and Transformer layers to analyze prostate MRI data for cancer identification, achieving high Accuracy and computational efficiency. Transformers effectively capture long-range tissue dependencies, but their quadratic memory growth becomes costly for high-resolution prostate images. To address this, Dimba replaces some Transformer attention layers with Mamba layers, improving computational throughput and reducing memory usage without compromising diagnostic quality. The core component, the Dimba Block, integrates Transformer attention with Mamba operations and a cross-attention mechanism that fuses MRI features with additional clinical or textual information, enabling contextually sensitive analysis of prostate cancer regions. Training follows a two-step process: large-scale pretraining on diverse prostate MRI datasets, followed by fine-tuning on carefully labelled cancer images. Quality adjustment aligns the model with medical-grade image distributions, improving segmentation precision and classification accuracy.

Additionally, Position Embedding smoothing enables the model to handle high-resolution prostate images efficiently, leading to faster convergence and more precise cancer boundary localization. The transform-Mamba synergy provides a balance of scalability, efficiency, and Accuracy, making Dimba a reliable framework for early prostate cancer detection and a practical decision-support tool for radiologists. The next section discusses the classification that follows feature extraction.

*E. Classification using Multi-Head ProbSparse Spherical Convolutional Network(M-HPSCNet)*

Classification enables precise decision-making by allocating extracted data or learning patterns into preset groups, such as cancerous compared to non-cancerous tissue. The MHPSCNet model is proposed for prostate cancer identification using MRI images, integrating two main components: the Multi-Head ProbSparse Self-Attention Network (MHPSAN)[25] and the Spherical Convolutional Neural Network (SCNN)[26]. MHPSAN emphasizes informative regions, eliminates irrelevant data, and captures complex structures, while SCNN leverages spherical feature modeling with reduced parameters, enhancing anomaly detection, region identification, and stage classification accuracy.

*a. Multi-Head Probsparse Self-Attention Network (MHPSAN)*

The MHPSAN enhances prostate cancer division and categorization by eliminating unnecessary information and focusing on the most instructive areas. By probabilistically distributing attention weights, it reduces computational cost and improves robustness over background noise and shifting imaging conditions. Multiple focus points that capture distinct feature subspaces enable the modelling of complex prostate cancer structures and disease patterns both locally and regionally. This approach preserves cancer borders, improves classification accuracy, and captures long-range feature associations, particularly in challenging MRI images. Equation (9) explains the sparsity metric for inquiries.

$$N(g_j, P) = 1m \sum_{j=1}^{K_L} d^{\frac{g_j P_i^H}{\sqrt{e}}} - \frac{1}{K_L} \sum_{j=1}^{K_L} \frac{g_j P_i^H}{\sqrt{e}} \quad (9).$$

where $g_j$ represents the $j - th$ query in the space of features, $P$ is the set of key vectors, $P_i$ indicates the $i - th$ key vector, $e$ provides the feature level for scaling dot-product similarities, $K_L$ represents the total number of keys, and $N(g_j, P)$ denotes the sparseness score for the $j - th$ query vector. $\sum_{j=1}^{K_L}$ Indicates the sum of all the essential vectors in the sequence, $1m$ is the logarithm of the total similarity scores, and $d^{\frac{g_j p_i^H}{\sqrt{e}}}$ is the exponential similarity between $g_j$ and $P_i$. Scaled dots product attention to prostate cancer extraction of features is explained by Equation (10).

$$Attention(K, Q, U) = softmax\left(\frac{\overline{K}Q^H}{\sqrt{e_p}}\right) \cdot U \quad (10).$$

Where $Q$ represents the query matrix, $K$ the key matrix, $U$ the value matrix, $\sqrt{e_p}$ the key dimension used for scaling, and $\overline{K}Q^H$ converts similarity scores. These operations allow the model to identify cancer-relevant regions in prostate

MRI images. **S** represents the similarity score matrix computed from the dot product of queries and keys. Equation (11) explains the multi-head ProbSparse Attention output for prostate cancer feature extraction.

$$Multihead(K,Q,U) = Concat(g_1, g_2, \cdots, g_m) \quad (11).$$

where the output of the $j-th$ attention head is represented by $g_1$, $m$ indicates the total number of attention heads, and the concatenation operation merges all head outputs into a single feature map, which is represented by $Concat$. This produces a cohesive feature representation, enabling the model to accurately delineate prostate cancer regions by capturing both global tissue structure and localized intensity patterns.

*b. A Spherical Convolutional Neural Network (SCNN)*

The SCNN utilizes Extended Gaussian Images (EGIs) to efficiently capture spatial domain oscillations in prostate MRI images for cancer diagnosis. Because SCNN combines circular harmonics and zonal kernels to reduce the number of learnable parameters while preserving strong feature representation, it is ideal for tiny medical datasets. This method provides a straightforward but effective alternative to conventional statistical or simulation-based photo analysis techniques. By modeling spatial information on spherical domains, SCNN enhances the detection of anomalies, stage classification, and region identification in prostate cancer image processing, ultimately improving diagnostic Accuracy. Equation (12) explains this process.

$$\hat{p}_n^K = \int_{x^2} r(y) N_m^K \, fx \quad (12).$$

where spherical functions of degree $n$ and order $K$ are used to depict the spatial distribution of the prostate MRI data. By projecting $fx$ into the unit sphere, $N_m^K$ it defines the detected region, signifying a particular cancerous spot. Spherical harmonic coefficients are indicated by $\hat{p}_n^K$, and feature traits are filtered by $r(y)$. To extract diagnostic data from the coefficients used in prostate cancer picture analysis, Equation (13) applies the inverse transform.

$$R = \sum_{0 \le n \le} R \sum_{|n| \le m} r_n^m Y_n^m \quad (13).$$

where, $R$ produces a uniform circular form that depicts a cancer zone, $Y$ stands for the general base integration, and $r_n^m$ indicates the harmony of the surface component for degrees $m$ $n$. Weighted basis averages that capture diagnosing patterns at various resolutions inside the spherical domain are indicated by numbers $\sum_{0 \le n \le} R$ and $\sum_{|n| \le m}$. The enlargement function for practical prostate cancer image analysis is shown in Equation (14).

$$D_G = \frac{\|D_k - D_p\|_G}{\|D_k\|_G} \quad (14).$$

where $D_p$ represents the approximation correlation matrix, $D_k$ denotes the real correlation matrix of cancer-related features, and $\| \ \|_G$ stands for the Frobenius norm. The error measure $D_G$ quantifies the difference between actual and predicted covariance values in prostate cancer image analysis. By combining spherical convolution and ProbSparse multi-head self-attention, M-HPSCNet enhances prostate cancer diagnosis in MRI by identifying both localized intensity fluctuations and global tissue features. This method guarantees accurate categorization even with tiny medical collections, lowers parameters, and enhances anomaly detection. LOA is used to increase the MHPSCNet weight parameters, which are denoted as $m$ and $n$.

*F. Lyrebird Optimization Algorithm (LOA)*

Optimization fine-tunes model parameters, hyperparameters, or processes, ensuring maximum Accuracy, efficiency, and generalization for medical image analysis tasks. The LOA[27] is a nature-inspired metaheuristic that is based on the Lyrebird's capacity to avoid danger. Exploration (escaping to safer regions) and exploitation (hiding in safe areas) are two survival strategies that it mimics. Candidate solutions represent lyrebirds in the search space where fitness values define safe places. Positions are updated through the use of escape and concealment techniques, enabling efficient local and global search. Because LOA avoids local optima and effectively balances exploration and exploitation, it is often employed in optimization tasks like determining controller parameters.

**Step 1: Initialization**

Initiate a population of lyrebirds and establish a maximum number of iterations. Each Lyrebird has a response. Equation (15) explains how positions are initialized.

$$T_b = (T_1, T_2, \cdots, T_P); (b = 1,2,..i,.., k) \quad (15).$$

where Lyrebird's location vector, represented by $T_b$, is one possible solution in the dimensional search space. $T_1$ Shows the Lyrebird's Position, $j - th$ dimension, and a particular attribute or parameter value that is essential to categorization precision. The current lyrebird population's index, $T$, ranges from $1\ to\ p$, where $p$ represents the overall amount of dimensions taken into account for optimization. Ultimately, $k$ represents the total number of lyrebirds, or alternative solutions, that have been randomly seeded to maximize classification performance and explore.

**Step 2: Fitness Function**

Employing a fitness function that indicates categorization performance, each Lyrebird's Position is assessed. The fitness function is explained by Equation (16).

$$Fitness\ function = Min(n, m)\ Max(Accuracy) \quad (16).$$

where $m$ represents the computing cost and $n$ denotes the error rate, both of which ought to be minimized. $Max(Accuracy)$ It can be utilized to emphasize a model's best performance while classifying image data.

**Step 3: Escape Behaviour**

During this phase, lyrebirds enhance their global search capabilities by updating their locations to enter safe zones. Equation (17) explains escape position updates.

$$g_{j,i}^{K1} = g_{j,i} + s_{j,i} \cdot (SSA_{j,i} - J_{j,i} \cdot g_{j,i}) \quad (17).$$

where $SSA_{j,i}$ denotes the $j - th$ Position of the chosen safe area, $s_{j,i}$ gives a random value that ranges from 0 to 1, and $g_{j,i}^{K1}$ displays the most significant recent Position for the $j - th$ Lyrebird in $i - th$ dimension. A randomly selected value, $J_{j,i}$, which can be either 1 or 2, determines the direction of progress in the position update.

**Step 4: Hiding Strategy**

Lyrebirds adjust their precise location within their environment to take advantage of the most popular choices. The hidden position update is explained by equation (18).

$$g_{j,i}^{K2} = g_{j,i} + (1 - 2s_{j,i}) \cdot \frac{vc_i - gc_i}{s} \quad (18).$$

where, $vc_i$ and $gc_i$ are the upper and lower bounds of the $i - th$ parameter, $g_{j,i}^{K2}$ and represent the updated location in $j - th$ dimension for the $i - th$ Lyrebird, respectively, and $s$ stands for the current iteration number.

**Step 5: Termination**

The process determines whether the maximum number of repetitions has been reached. If not, the process goes back to the investigation stage and modifies the overall number of iterations $i = i + 1$. When the maximum number of iterations is reached, the technique selects the optimal alternative with the lowest error in reconstruction and the highest classification accuracy. LOA aims to effectively adjust the model variables and hyperparameters to maximize classification accuracy while lowering computing cost and error. To balance local exploitation with global exploration in the search space, it imitates lyrebird survival techniques. Figure 2 provides the LOA.

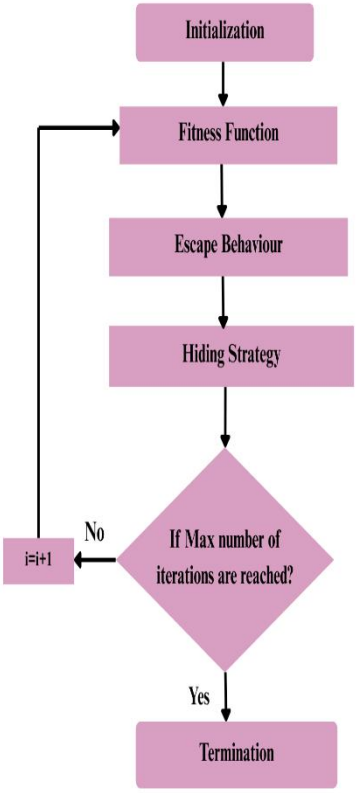


**Fig.2. Flow chart for Lyrebird Optimization Algorithm**

## 4. RESULTS AND DISCUSSION

The proposed method utilizes the SCNN neural network, which was developed from the SPIE-AAPM-NCI Prostate dataset and optimized using the LOA. The NVIDIA GeForce RTX 2060 GPU (4 GB), an Intel Core i7-10750H processor, 16 GB DDR4 RAM, and a 500 GB SSD have been evaluated using Python v3. Table 1 provides a summary of the model and implementation parameters.

**TABLE I. IMPLEMENTATION PARAMETERS**

| **Parameters** | **Values** |
|---|---|
| Neural Network | SCNN |
| Dataset | SPIE-AAPM-NCI Prostate |
| Optimization | Lyrebird Optimization Algorithm |
| GPU | NVIDIA GeForce RTX 2060, 4 GB |
| Processor | Intel Core i7-10750H, 10th Gen, Base Clock 2.6 GHz, Turbo Boost up to 5.0 GHz |
| RAM | 16 GB DDR4, 2666 MHz |
| Storage | 500 GB SSD |
| Programming Language | Python v3 |

*A. Dataset description*

The SPIE-AAPM-NCI Prostate dataset[8] MRI image comprises 346 patients with PI-RADS scores ≥3, including T2-Weighted (T2W), Dynamic Contrast-Enhanced (DCE), Proton Density-Weighted (PD-W), and Diffusion-Weighted (DW) MRI series. Each patient has multiple DICOM images and one Ktrans image, totaling 309,251 images (15.1 GB) across

18,321 series. The dataset is labeled for binary classification: Prostate Cancer (GG ≥3, Gleason Score ≥7) and Non-Cancer (GG <3). The training set contains 112 lesions, and the testing set contains 70 lesions. Lesion locations and Gleason Grades are recorded in Excel files. For this study, 56 MRI images—32 T2W, 12 Ktrans, and 12 ADC—are used.

*B. Performance Analysis of Proposed Model*

The effectiveness of the proposed method is evaluated using the SPIE-AAPM-NCI Prostate dataset, with a focus on features that are critical for accurate cancer identification. Model performance is assessed using F1-score, Accuracy, precision, recall, and specificity. The results demonstrate the method's excellent Accuracy in detecting prostate cancer lesions, high consistency during training, and reliable assistance for classification and diagnostic analysis.

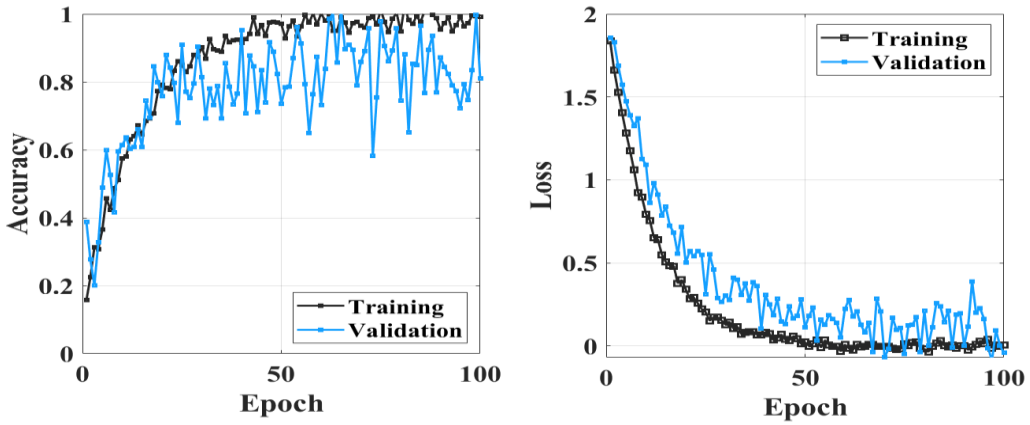


**(a)** **(b)**

Fig.3. Proposed (a) Accuracy and (b) Loss for SPIE-AAPM-NCI Prostate Dataset

Figure 3 demonstrates the suggested model's performance during training and validation on the SPIE-AAPM-NCI dataset. While loss continuously declines, Accuracy gradually rises to almost 1. This shows good generalization ability, consistent convergence, decreased prediction error, and efficient learning for MRI-based prostate cancer diagnosis.

*C. Comparative analysis*

The efficiency of the suggested MHPSCNet-LOA technique for prostate cancer diagnosis is assessed using the SPIE-AAPM-NCI Prostate dataset. Specificity, Accuracy, recall, precision, and F1-score are the primary performance measures taken into account. The comparison results against other approaches, such as 3D CNN [8], Residual Network (RN) [9], DeepLabv3+ [10], and SVM [11], are shown in Table 2.

**TABLE II. PERFORMANCE COMPARISON ON THE SPIE-AAPM-NCI PROSTATE DATASET**

| **Methods** | **Accuracy (%)** | **Precision (%)** | **F1-score (%)** | **Recall (%)** | **Specificity (%)** |
|---|---|---|---|---|---|
| 3D CNN [8] | 86 | 77 | 72 | 13 | 12 |
| Residual Network (RN) [9] | 87 | 81 | 88 | 16 | 17 |
| DeepLabv3+ [10] | 84 | 79 | 89 | 17 | 13 |
| SVM [11] | 86 | 84 | 85 | 19 | 10 |
| **MHPSCNet-LOA (proposed)** | 99.85 | 99.62 | 99.58 | 0.3 | 0.2 |

Table 2 evaluates the effectiveness of various methods for identifying prostate cancer. Accuracy ranges from 84 to 87% for traditional models with moderate Accuracy and F1-scores, including 3D CNN, RN, DeepLabv3+, and SVM. However, the proposed MHPSCNet-LOA achieves 99.85% accuracy, 99.62% precision, and 99.58% F1-score, outperforming existing deep learning methods in terms of resilience, diagnostic reliability, and Accuracy.

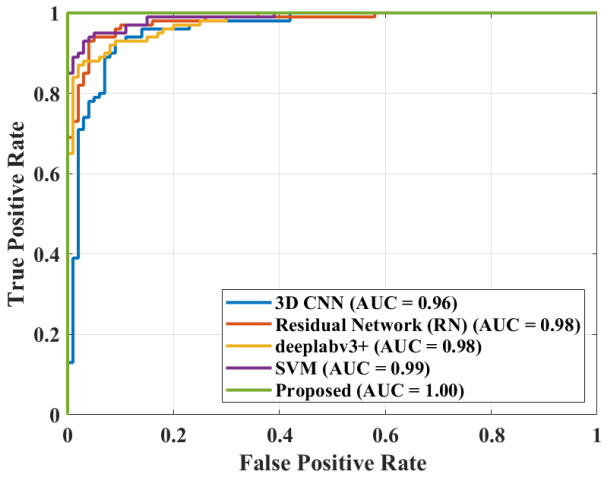


Fig.4. ROC Curve Comparison of Different Methods on SPIE-AAPM-NCI Prostate Dataset

Figure 4 shows the ROC curve, which contrasts the classification performance of several models. The recommended method outperforms 3D CNN, RN, DeepLabv3+, and SVM in terms of sensitivity, specificity, and durability for MRI image-based prostate cancer diagnosis, achieving an AUC of 1.00.

## 5. CONCLUSION

The proposed Multi-Head ProbSparse Spherical Convolutional Network with Lyrebird Optimization Algorithm (M-HPSCNet-LOA) presents a robust and intelligent framework for prostate cancer detection from the SPIE-AAPM-NCI Prostate dataset using MRI images. By integrating Deep Attentional Guided Image Filtering for effective pre-processing, Single-Head Vision Transformer for accurate segmentation, Dimba (TMDM) for efficient feature extraction, and a hybrid classification model combining ProbSparse Self-Attention with Spherical Convolutional Neural Networks, the approach captures both global structural patterns and localized tumor-specific details. The incorporation of the Lyrebird Optimization Algorithm further enhances the system by fine-tuning model parameters and preventing convergence to local optima, thereby achieving improved stability and Accuracy. Experimental evaluation on the SPIE-AAPM-NCI dataset demonstrates outstanding performance, with an accuracy of 99.85%, precision of 99.62%, and F1-score of 99.58%, surpassing existing deep learning and traditional approaches. The advantages of this framework include strong diagnostic reliability, efficient representation of prostate tissue features, and adaptability through optimized learning strategies. Nonetheless, the model has limitations, particularly its dependence on high computational resources, validation on a single dataset, and limited interpretability for direct clinical use. Future research will address these challenges by testing across larger and diverse datasets, incorporating explainable AI techniques, reducing computational complexity, and extending applicability to multimodal analysis and other cancer types.

## REFERENCES

[1] M. E. Salman, G. Ç. Çakar, J. Azimjonov, M. Kösem, and İ. H. Cedimoğlu, “Automated prostate cancer grading and diagnosis system using deep learning-based Yolo object detection algorithm,” Expert Syst. Appl., vol. 201, p. 117148, 2022. DOI: 10.1016/j.eswa.2022.117148

[2] A. M. Alshareef, R. Alsini, M. Alsieni, F. Alrowais, R. Marzouk, I. Abunadi, et al., “Optimal deep learning enabled prostate cancer detection using microarray gene expression,” J. Healthc. Eng., vol. 2022, no. 1, p. 7364704, Mar. 10 2022. DOI: 10.1155/2022/7364704

[3] M. R. Hassan, M. F. Islam, M. Z. Uddin, G. Ghoshal, M. M. Hassan, S. Huda, et al., “Prostate cancer classification from ultrasound and MRI images using deep learning based Explainable Artificial Intelligence,” Future Gener. Comput. Syst., vol. 127, pp. 462–472, 2022. DOI: 10.1016/j.future.2021.09.030

[4] S. Mehralivand, D. Yang, S. A. Harmon, D. Xu, Z. Xu, H. Roth, et al., “Deep learning-based artificial intelligence for prostate cancer detection at biparametric MRI,” Abdom. Radiol. (N.Y.), vol. 47, no. 4, pp. 1425–1434, Apr. 2022. DOI: 10.1007/s00261-022-03419-2

[5] F. M. Talaat, S. El-Sappagh, K. Alnowaiser, and E. Hassan, “Improved prostate cancer diagnosis using a modified ResNet50-based deep learning architecture,” BMC Med. Inform. Decis. Mak., vol. 24, no. 1, p. 23, Jan. 24 2024. DOI: 10.1186/s12911-024-02419-0

[6] S. Deng, J. Ding, H. Wang, G. Mao, J. Sun, J. Hu, et al., “Deep learning-based radiomic nomograms for predicting Ki67 expression in prostate cancer,” BMC Cancer, vol. 23, no. 1, p. 638, Jul. 8 2023. DOI:

10.1186/s12885-023-11130-8

[7] M. M. Behzadi, M. Madani, H. Wang, J. Bai, A. Bhardwaj, A. Tarakanova, et al., "Weakly-supervised deep learning model for prostate cancer diagnosis and Gleason grading of histopathology images," Biomed. Signal Process. Control, vol. 95, p. 106351, 2024. DOI: 10.1016/j.bspc.2024.106351

[8] Talaat, F.M., El-Sappagh, S., Alnowaiser, K. and Hassan, E., 2024. Improved prostate cancer diagnosis using a modified ResNet50-based deep learning architecture. BMC Medical Informatics and Decision Making, 24(1), p.23.

[9] Alzboon, M.S. and Al-Batah, M.S., 2023. Prostate cancer detection and analysis using advanced machine learning. International Journal of Advanced Computer Science and Applications, 14(8).

[10] Salman, M.E., Çakar, G.Ç., Azimjonov, J., Kösem, M. and Cedimoğlu, İ.H., 2022. Automated prostate cancer grading and diagnosis system using deep learning-based Yolo object detection algorithm. Expert Systems with Applications, 201, p.117148.

[11] Bhattacharya, I., Seetharaman, A., Kunder, C., Shao, W., Chen, L.C., Soerensen, S.J., Wang, J.B., Teslovich, N.C., Fan, R.E., Ghanouni, P. and Brooks, J.D., 2022. Selective identification and localization of indolent and aggressive prostate cancers via CorrSigNIA: an MRI-pathology correlation and deep learning framework. Medical image analysis, 75, p.102288.

[12] Wang, Y., Ji, B., Zhang, L., Wang, J., He, J., Ding, B. and Ren, M., 2024. Identification of metastasis-related genes for predicting prostate cancer diagnosis, metastasis and immunotherapy drug candidates using machine learning approaches. Biology Direct, 19(1), p.50.

[13] Hassan, M.R., Islam, M.F., Uddin, M.Z., Ghoshal, G., Hassan, M.M., Huda, S. and Fortino, G., 2022. Prostate cancer classification from ultrasound and MRI images using deep learning based Explainable Artificial Intelligence. Future Generation Computer Systems, 127, pp.462-472.

[14] Moroianu, Ş.L., Bhattacharya, I., Seetharaman, A., Shao, W., Kunder, C.A., Sharma, A., Ghanouni, P., Fan, R.E., Sonn, G.A. and Rusu, M., 2022. Computational detection of extraprostatic extension of prostate cancer on multiparametric MRI using deep learning. Cancers, 14(12), p.2821.

[15] Michaely, H.J., Aringhieri, G., Cioni, D. and Neri, E., 2022. Current value of biparametric prostate MRI with machine-learning or deep-learning in the detection, grading, and characterization of prostate cancer: a systematic review. Diagnostics, 12(4), p.799.

[16] Harder, F.N., Weiss, K., Amiel, T., Peeters, J.M., Tauber, R., Ziegelmayer, S., Burian, E., Makowski, M.R., Sauter, A.P., Gschwend, J.E. and Karampinos, D.C., 2022. Prospectively accelerated T2-weighted imaging of the prostate by combining compressed SENSE and deep learning in patients with histologically proven prostate cancer. Cancers, 14(23), p.5741.

[17] Singh, S.K., Sinha, A., Singh, H., Mahanti, A., Patel, A., Mahajan, S., Pandit, A.K. and Varadarajan, V., 2024. A novel deep learning-based technique for detecting prostate cancer in MRI images. Multimedia Tools and Applications, 83(5), pp.14173-14187.

[18] S. K. Singh, A. Sinha, H. Singh, A. Mahanti, A. Patel, S. Mahajan, et al., "A novel deep learning-based technique for detecting prostate cancer in MRI images," Multimedia Tools Appl., vol. 83, no. 5, pp. 14173–14187, 2024. DOI: 10.1007/s11042-023-15793-0

[19] A. Horasan and A. Güneş, "Advancing prostate cancer diagnosis: A deep learning approach for enhanced detection in MRI images," Diagnostics (Basel), vol. 14, no. 17, p. 1871, Aug. 27 2024. DOI: 10.3390/diagnostics14171871

[20] T. Yoshimura, K. Manabe, and H. Sugimori, "Non-Invasive Estimation of Gleason Score by Semantic Segmentation and Regression Tasks Using a Three-Dimensional Convolutional Neural Network," Appl. Sci. (Basel), vol. 13, no. 14, p. 8028, 2023. DOI: 10.3390/app13148028

[21] S. T. Alanezi, M. J. Kraśny, C. Kleefeld, and N. Colgan, "Differential diagnosis of prostate cancer grade to augment clinical diagnosis based on classifier models with tuned hyperparameters," Cancers (Basel), vol. 16, no. 11, p. 2163, Jun. 6 2024. DOI: 10.3390/cancers16112163

[22] Z. Zhong, X. Liu, J. Jiang, D. Zhao, and X. Ji, "Deep attentional guided image filtering," IEEE Trans. Neural Netw. Learn. Syst., 2023.

[23] S. Yun and Y. Ro, 2024. Shvit: Single-head vision transformer with memory efficient macro design. In Proceedings of the IEEE/CVF Conference on Computer Vision and Pattern Recognition (pp. 5756-5767). DOI: 10.1109/CVPR52733.2024.00550

[24] Z. Fei, M. Fan, C. Yu, D. Li, Y. Zhang, and J. Huang, 2024. Dimba: Transformer-mamba diffusion models. arXiv preprint arXiv:.

[25] Y. Zhang, H. Wu, J. Xian, X. Mei, K. Zhang, Q. Zhang, et al., "A Multi-head ProbSparse Self-attention Mechanism based High-Precision and High-Robustness Reconstruction Model for Missing Ocean Data," IEEE Sens. J., 2025.

[26] F. Sinzinger, J. van Kerkvoorde, D. H. Pahr, and R. Moreno, "Predicting the trabecular bone apparent stiffness tensor with spherical convolutional neural networks," Bone Rep., vol. 16, p. 101179, Mar. 7 2022. DOI: 10.1016/j.bonr.2022.101179

[27] A. M. El-Rifaie, "A novel lyrebird optimization algorithm for enhanced generation rate-constrained load frequency control in multi-area power systems with proportional integral derivative controllers," Processes (Basel), vol. 13, no. 4, p. 949, 2025. DOI: 10.3390/pr13040949